Cambridge Centre for Computational Chemical Engineering

University of Cambridge

Department of Chemical Engineering

Preprint ISSN 1473 – 4273

Coupling a stochastic soot population balance to gas-phase chemistry using operator splitting

Matthew Celnik, Robert Patterson, Markus Kraft [1] ,

Wolfgang Wagner [2]

released: 23 May 2006

[1] Department of Chemical Engineering
University of Cambridge
Pembroke Street
Cambridge CB2 3RA
UK
E-mail: mk306@cam.ac.uk

[2] Weierstrass Institute for
Applied Analysis and Stochastics
Mohrenstraße 39
D-10117 Berlin
Germany

Preprint No. 39

c4e

Key words and phrases: soot, stochastic, operator splitting, Strang splitting, numerical convergence, particle composition

Edited by
Cambridge Centre for Computational Chemical Engineering
Department of Chemical Engineering
University of Cambridge
Cambridge CB2 3RA
United Kingdom.

Fax: + 44 (0)1223 334796
E-Mail: c4e@cheng.cam.ac.uk
World Wide Web: http://www.cheng.cam.ac.uk/c4e/

Abstract

The feasibility of coupling a stochastic soot algorithm to a deterministic gas-phase chemistry solver is investigated for homogeneous combusting systems. A second order splitting technique was used to decouple the particle population and gas-phase in order to solve. A numerical convergence study is presented which demonstrates convergence with splitting step size and particle count for a batch reactor and a perfectly stirred reactor (PSR). Simulation results are presented alongside experimental data for a plug flow reactor (PFR) and a comparison to a method of moments simulation of a perfectly stirred reactor. Coupling of the soot and chemistry solvers is shown to converge for both systems, however, numerical instabilities present significant challenges in the PSR case. Comparison with the experimental data for a PFR showed good agreement of the soot mass, and reasonable agreement of the particle size distribution. Two different soot particle models were used to simulate the PFR; a spherical particle model and a surface-volume model which takes some account of particle shape. The results for both models are compared. Additionally the stochastic soot solver is used to track the evolution of the C/H ratio of individual soot particles in the PFR for the first time.

Contents

1 Introduction

The formation of fine particulate matter in hydrocarbon flames is an important industrial and environmental process. Soot particles are produced in industrial carbon-black processes as pigments for inks, although the primary focus on soot particle formation is the environmental sector. There is a popular drive towards lower emission technology, especially for road and air transport, and large scale combustors. Soot particulates and their precursors, Polycyclic Aromatic Hydrocarbons (PAHs) are major health and environmental hazards, and it is generally acknowledged that their reduction would be beneficial.

A first step towards soot reduction is to understand the mechanisms by which soot is formed. The present understanding of the processes leading to soot production in combusting systems is limited. Combusting systems, such as premixed laminar flames, are very difficult to observe experimentally, due to the short time scales of the processes (nanoseconds) and the general complexity of the chemical interactions. Therefore, computer simulations are important tools for investigation of such environments, in particular for the soot particle size distribution.

Simulation of soot particle formation in flames requires detailed models for the gas-phase chemistry, soot particle chemistry and inter-particle interactions. Wang et al. [24] proposed a detailed reaction mechanism to describe aromatics formation in acetylene (C_2H_2) and ethylene flames. This mechanism was later improved by Appel et al. [1] to give the ABF chemistry model. The ABF soot model was used exclusively for this work. PAHs are considered to be the main precursors for soot formation [1], and of those pyrene is thought to be the most important. The Hydrogen Abstraction Carbon Addition (HACA) mechanism [10] is considered an important growth mechanism for PAHs and soot particles. Through this mechanism, aromatics and soot particles grow by the addition of growth species, principally acetylene, to active sites on the particle surface - carbon addition. An active site is a point where a hydrogen atom has been removed - the hydrogen abstraction step. In [9] it was demonstrated that, by performing a steady-state analysis on the HACA reactions, the ratio of active sites to active radical sites on a soot particle could be found. The fraction of surface sites which are active is denoted everywhere as α. Expressions for α are a matter of much debate, and for this report the correlation of [1] was used, which models α as a function of the gas-phase temperature and mean particle size, and was fitted for laminar premixed flames.

In order to solve both the gas-phase chemistry and the soot population balance, a method for relating the two systems must be obtained. This is not straightforward, as the soot population can contain many millions of particles with different properties. Tracking every particle is currently computationally impossible within realistic time scales. A reduced representation of the soot population is required in order to solve it numerically. The method of moments with interpolative closure (MoMIC, referred to as method of moments) [8] was proposed as a technique for describing a soot population by a handful of variables; the moments of the distribution. The method of moments has the advantage of being fast, as typically balances for only six moments are solved, and these can be solved using the same ODE solver as the gas-phase chemistry equations. However, the method of moments requires an extrapolation to find additional moments and gives no information about the shape of the particle size distribution (PSD). Galerkin methods [2]

and fixed [20] or moving [26] sectional techniques have been used to describe a soot population with some degree of resolution of the PSD, although these techniques suffer from numerical diffusion and are computationally more intensive than the method of moments.

Monte-Carlo techniques have been applied to the solution of soot population balances [3]. These techniques can provide much more information about the soot population and the development of soot particles as they avoid the approximations made for process rates in Galerkin and sectional techniques. Monte-Carlo simulations can be proven to converge to the deterministic solution of the population balance equations [7]. However, they can be computationally very expensive and they provide no capacity for solving the gas-phase chemistry deterministically. In [3] Balthasar and Kraft solved laminar premixed flames by solving the flame chemistry deterministically using the method of moments to approximately account for the effects of soot. They used the generated chemical species profiles as inputs to their stochastic soot solver and a Direct Simulation Monte-Carlo algorithm (DSMC) which models every soot event explicitly within the soot ensemble. [18] further improved this technique with the Linear Process Deferment Algorithm (LPDA) which significantly reduces computation time, while giving rise to only negligible additional error.

The **purpose of this paper** is to present a second order operator splitting technique for coupling a stochastic soot model to gas-phase chemistry for spatially homogeneous initial value problems. A description of the technique is provided along with the governing equations, and the numerical treatment is explained. The technique is used to simulate a Plug-Flow Reactor (PFR) and a Perfectly Stirred Reactor (PSR). For the PFR the results of particle diameter, mass and distribution are compared to experimental data. For the first time the Carbon to Hydrogen (C/H) ratio of individual particles is tracked in the PFR, and the time evolution of the C/H ratio is presented.

The paper is organised as follows. First the governing for a batch reactor (including a PFR) and a PSR are presented along with any assumptions. The operator splitting algorithm is then discussed. Next a numerical convergence study is presented for both a batch reactor and a PSR. The technique is then compared to experimental observations of a PFR, and time evolutions of the C/H ratio are presented for two different particle models. A numerical comparison is made between an operator splitting simulation and a method of moments simulation for a PSR. The paper closes with a discussion of the technique's viability and application.

2 Model

The gas phase is modelled using the model of [1] and is assumed to obey the ideal gas law. The gas-phase model contains 101 species and 544 reactions. Chemical reaction rates in the gas-phase are modelled as Arrhenius form.

Soot particles are assumed to be homogeneous with a density of $\rho_s = 1.8\ \mathrm{kg/m^3}$. A soot particle is considered to be any carbon structure with at least 32 carbon atoms. Two models of particle shape were used. One, the spherical particle model [3, 22], treats all particles as spheres described by their volume. The second, the surface-volume model

[19], attempts to account for particle shape by introducing an extra variable, surface area, which is independent of volume. Both models were extended to track the ratio of carbon to hydrogen in each particle.

Two constant pressure reactor models were implemented; a batch reactor and a PSR. The PSR is similar to the batch reactor, but with inflow and outflow. The gas-phase chemistry requires the solution of each species concentration and the temperature; that is $K + 1$ variables, where K is the number of gas-phase species. The soot particle population evolves according to the discrete Smoluchowski equation. Two energy regimes were considers; constant temperature and adiabatic. Energy terms associated with soot processes (radiation and formation) were found to be negligible for the cases studied and hence were neglected.

The governing equations (gas-phase material balance and soot population balance) for a constant pressure batch reactor are:

$$\frac{dc_k}{dt} = \dot{\omega}_k(c, T) + \dot{g}_k(c, n, T) - \gamma c_k \tag{1}$$

$$\frac{d}{dt}n(x) = I(c, x) + K(n, x) + \sum_{l=1}^{L} S_l(c, x) - \gamma n(x) \tag{2}$$

Where c_k is the molar concentration of species k, $\dot{\omega}_k$ is the molar production rate of species k due to reaction, $\dot{g}_k$ is the molar production rate of species k due to soot processes, and T is the temperature. In the soot balance $n(x)$ is the number density of particles of type x, where the type is a vector of particle volume, composition, and surface area (surface-volume model only). $I(c, x)$, $K(n, x)$ and $S_l(c, x)$ are the inception, coagulation and surface reaction l rates respectively for particles of type x. c denotes the vector of species concentrations. γ is the rate of gas-phase expansion and is given by:

$$\gamma = \frac{\dot{\omega}_k}{\rho} + \frac{1}{T}\frac{dT}{dt} \tag{3}$$

where ρ is the molar density of the bulk fluid. Note the molar production rate due to soot is considered small in magnitude compared to that due to chemical reaction. The adiabatic energy balance for a batch reactor (ignoring soot energy terms) yields:

$$\rho\hat{C}_p\frac{dT}{dt} = -\sum_{k=1}^{K}\bar{H}_k\dot{\omega}_k \tag{4}$$

where $\hat{C}_p$ is the molar heat capacity of the mixture and $\bar{H}_k$ is the partial molar enthalpy of species k.

For a constant pressure PSR the further assumptions were made that no soot particles are present in the inflow, the inflow and outflow volumetric flows are equal and the residence

time is constant. Therefore, the governing equations for a PSR are:

$$\frac{dc_k}{dt} = \dot{\omega}_k(c,T) + \dot{g}_k(c,n,T) + \frac{1}{\tau}(c_{k0} - c_k) - \gamma c_k \tag{5}$$

$$\frac{d}{dt}n(x) = I(c,x) + K(n,x) + \sum_{l=1}^{L} S_l(c,x) - \frac{n(x)}{\tau} - \gamma n(x) \tag{6}$$

Where τ is the reactor residence time, and subscript 0 denotes inflowing material. The rate of gas-phase expansion for a PSR is given by:

$$\gamma = \frac{1}{\rho}\left(\dot{\omega}_k + \frac{1}{\tau}(\rho_0 - \rho)\right) + \frac{1}{T}\frac{dT}{dt} \tag{7}$$

The adiabatic energy balance for a PSR (ignoring soot energy terms) is:

$$\rho\hat{C}_p\frac{dT}{dt} = -\sum_{k=1}^{K}\bar{H}_k\dot{\omega}_k + \frac{1}{\tau}\sum_{k=1}^{K}c_{k0}(\bar{H}_{k0} - \bar{H}_k) \tag{8}$$

3 Numerical Treatment

3.1 Splitting Scheme

Representing the soot ensemble as a list of particle concentrations is unrealistic as there is an infinite space of possible particle types. The soot ensemble is therefore represented as a discrete list of particles, and is solved using an explicit Monte-Carlo technique. The gas-phase chemistry is best solved using an implicit ODE solution technique, as there are only a finite number of gas-phase variables (chemical species and temperature). An operator splitting technique was used to solve the two parts of the problem separately. For the batch reactor the governing equations can be split term-wise so that all terms with no soot dependency are collected separately from those with soot dependency:

$$\frac{dc_k}{dt} = \dot{\Omega}_k(c,T) + \dot{g}_k(c,n,T) \tag{9}$$

$$\frac{d}{dt}n(x) = -\gamma(c,T)n(x) + \Psi(c,n,x,T) \tag{10}$$

$$\frac{dT}{dt} = \Theta(c,T) \tag{11}$$

Where:

$$\dot{\Omega}_k(c,T) = \dot{\omega}_k(c,T) - \gamma(c,T)c_k \tag{12}$$

$$\Psi(c, n, x, T) = I(c, x) + K(n, x) + \sum_{l=1}^{L} S_l(c, x) \tag{13}$$

$$\Theta(c, T) = -\frac{1}{\rho \hat{C}_p} \sum_{k=1}^{K} \bar{H}_k \dot{\omega}_k \tag{14}$$

Both a batch reactor and a PSR are initial value problems. We wish to find the values at the end of one time step, $t_1 = t_0 + h$. Using a simple operator splitting technique over the time step this can be solved in two stages. First solve using the ODE solver, and then using the Monte-Carlo solver. A further refinement is gained by using the method from [23], which was shown to be second order accurate. The method staggers the two solvers by half a step. The splitting scheme is then solved as follows:

ODE solver:

$$\begin{aligned}
\frac{d}{dt} c_k'(t) &= \Omega(c', T') \,, \quad c'(t_0) = c(t_0) \,, \quad t_0 \le t \le t_0 + \frac{h}{2} \\
\frac{d}{dt} n'(x,t) &= -\gamma(c', T')\, n'(x,t) \,, \quad n'(x, t_0) = n(x, t_0) \,, \quad t_0 \le t \le t_0 + \frac{h}{2} \\
\frac{d}{dt} T'(t) &= \Theta(c', T') \,, \quad T'(t_0) = T(t_0) \,, \quad t_0 \le t \le t_0 + \frac{h}{2}
\end{aligned} \tag{15}$$

Monte-Carlo solver:

$$\begin{aligned}
\frac{d}{dt} c_k''(t) &= \dot{g}_k(c'', n'', T'') \,, \quad c''(t_0) = c'\left(t_0 + \frac{h}{2}\right) \,, \quad t_0 \le t \le t_1 \\
\frac{d}{dt} n''(x,t) &= \Psi(c'', n'', T'') \,, \quad n''(x, t_0) = n'\left(x, t_0 + \frac{h}{2}\right) \,, \quad t_0 \le t \le t_1 \\
\frac{d}{dt} T''(t) &= 0 \,, \quad T''(t_0) = T'\left(t_0 + \frac{h}{2}\right) \,, \quad t_0 \le t \le t_1
\end{aligned} \tag{16}$$

ODE solver:

$$\begin{aligned}
\frac{d}{dt} c_k'''(t) &= \Omega(c''', T''') \,, \quad c'''\left(t_0 + \frac{h}{2}\right) = c''(t_1) \,, \quad t_0 + \frac{h}{2} \le t \le t_1 \\
\frac{d}{dt} n'''(x,t) &= -\gamma(c''', T''')\, n'''(x,t) \,, \quad n'''\left(x, t_0 + \frac{h}{2}\right) = n''(x, t_1) \,, \quad t_0 + \frac{h}{2} \le t \le t_1 \\
\frac{d}{dt} T'''(t) &= \Theta(c''', T''') \,, \quad T'''\left(t_0 + \frac{h}{2}\right) = T''(t_0) \,, \quad t_0 + \frac{h}{2} \le t \le t_1
\end{aligned} \tag{17}$$

Finally assign the values at the step end point:

$$
\begin{aligned}
c(t_1) &= c'''(t_1) \\
n(x,t_1) &= n'''(x,t_1) \\
T(t_1) &= T'''(t_1)
\end{aligned}
\tag{18}
$$

Strang splitting is particularly advantageous as, except for the initial and final half chemistry steps, the algorithm is the same as for simple splitting when multiple steps are performed at once: Solve using Monte-Carlo for one step, then solve using the ODE solver for one step. This means that the computation time is effectively the same for both methods, yet Strang splitting reduces the splitting error.

3.2 Method

The chemical kinetics were solved using the CHEMKINII suite of routines, which were written to solve large chemical mechanisms. A proprietary ODE solver was chosen to solve the gas-phase chemistry equations. The soot solver reported in [18], SWEEP, was used to solve the soot population balance and corresponding gas-phase chemistry terms. The algorithm [18] was extended to track the gas-phase chemistry changes due to soot processes and the particle type was extended to track particle composition.

Two ODE solvers were considered to solve chemistry equations; RADAU5 [12] and DDASSL [4]. RADAU5 solves a system of ODEs using a fifth order Runge-Kutta method. DDASSL uses a backwards-differentiation scheme of orders one through five. Potential problems identified with all high-precision ODE solvers are initialisation time, and accuracy/stability of solution. Both RADAU5 and DDASSL are in the public domain, are well established and are widely used [6]. RADAU5 has the advantage of lower run times, in particular initialisation time, though it was found not always to be stable for the systems of interest. DDASSL is very stable and can achieve high accuracy, however, it suffers from long initialisation times. The splitting algorithm requires the ODE solver to be reset each time the Monte-Carlo solver is run in order to recalculate higher order derivatives used in the integration, therefore initialisation time is an important factor in determining the computational speed of the method. For this reason RADAU5 was chosen in preference to DDASSL.

4 Numerical Convergence

There are three numerical parameters within the algorithm which affect the numerical error. These are the maximum number of particles in the stochastic simulation (N_{max}), the number of independent trials or runs (L) and the splitting time-step size (Δt). The effect of these parameters on the numerical error was investigated.

The systematic (e_{sys}) and statistical (e_{stat}) errors of a set of sample solutions ($y(t)$) are defined as follows:

$$\begin{aligned} e_{sys}(t) &= |\zeta(t) - F(t)| \\ e_{stat}(t) &= |\eta_y(t) - \zeta(t)| \end{aligned} \tag{19}$$

where $\zeta(t)$ is the expectation of the distribution from which $y_l(t)$ is sampled and F is the true solution. $\eta_y(t)$ is the estimate of the mean value, and is given by:

$$\eta_y(t) = \frac{1}{L}\sum_{l=1}^{L} y_l(t) \tag{20}$$

The true solution to the original problem is not readily obtainable, therefore a numerical solution for which the systematic error is very small ($\tilde{F}$) was selected as an approximation to the solution. The systematic error due to the Monte-Carlo algorithm is shown to become small when the approximation parameter, N, becomes very large [7].

For large L the central limit theorem may be used to find confidence intervals for $\eta_y(t)$. The half widths of these are estimated by:

$$c_p(t) = a_p\sqrt{\frac{\mu_y(t)}{L}} \tag{21}$$

where $\mu_y(t)$ is the approximation of the variance and is given by:

$$\mu_y(t) = \frac{1}{L-1}\sum_{l=1}^{L} y_l^2(t) - [\eta_y(t)]^2 \tag{22}$$

For a confidence level of $P = 0.999$ (99.9%), a value $a_p = 3.29$ is used. The confidence interval, within which there is a probability P of finding the true solution, is then given by:

$$I_p = [\eta_y - c_p,\ \eta_y + c_p] \tag{23}$$

In order to assess the numerical convergence of the coupled algorithm three test functions were chosen. These were particle number density (M_0), soot volume fraction (F_v) and pyrene concentration (c_{pyr}). For the purposes of this study, representative total relative errors (c_{tot}) and relative statistical uncertainties (c_{stat}) over M time intervals were calculated. t_m is the time at the end of interval m where $m \in \{0, 1, ..., M\}$.

$$c_{tot} = \frac{1}{M}\sum_{m=1}^{M} \frac{|\tilde{F}(t_m) - \eta_y(t)|}{\tilde{F}(t_m)} \tag{24}$$

$$c_{stat} = \frac{1}{M}\sum_{m=1}^{M} \frac{c_p(t_m)}{\tilde{F}(t_m)} \tag{25}$$

The numerical convergence was investigated as both splitting step count M and maximum stochastic particle count N_{max} were altered. A variable particle count algorithm was used along with a particle doubling algorithm [21] so that the actual particle count lay in the range $\left[\frac{1}{2}N_{max}, N_{max}\right]$ except at early flow times.

4.1 Batch Reactor

A simple test case was created in order to perform a numerical convergence study for a batch reactor. The test case was a initial $C_2H_2/O_2/N_2/Ar$ mixture of equivalence ratio $\phi = 2.5$. The temperature was assumed to be constant at 1650 K and the pressure was chosen as 1 atm. No particles were present in the reactor initially and the run time was 50 ms. The spherical particle model was used for this study. The simulations are listed in table 1.

Table 1: *Batch reactor numerical convergence simulations*

Simulation	M	L	N_{max}	Simulation	M	L	N_{max}
1	100	400	2048	11	300	12800	64
2	200	400	2048	12	300	6400	128
3	300	400	2048	13	300	3200	256
4	400	400	2048	14	300	1600	512
5	500	400	2048	15	300	800	1024
6	600	400	2048	16	300	400	2048
7	700	400	2048	17	300	200	4096
8	800	400	2048	18	300	100	8192
9	900	400	2048	19	300	50	16384
10	1000	400	2048	20	300	25	32768
				21	300	13	65536
Reference Case					2000	50	131072

The total error and statistical uncertainties for the three test functions are plotted in figure 1. The figure also shows a least squares power law fit of the data, and unfitted slopes indicating what second order convergence would look like. There is a clear reduction in total error as the number of splitting steps is increased and hence the technique has been shown to converge in this instance. Increasing the stochastic particle count has negligible effect on the error, even at very small particle counts, demonstrating that the Monte-Carlo part of the algorithm used enough particles in all cases to avoid significant systematic error. It is interesting to note that while Strang suggested a second order convergence for decreasing step count, the least squares fits show orders around 1.2. This is consistent with the findings of [27]. Also from figure 1 it can be seen that the F_v error begins to flatten at higher step counts, within the statistical uncertainty bounds, and further increases make no difference to the error. This demonstrates that F_v has converged sufficiently to become insensitive to step size and the error is dominated by the statistical fluctuations.

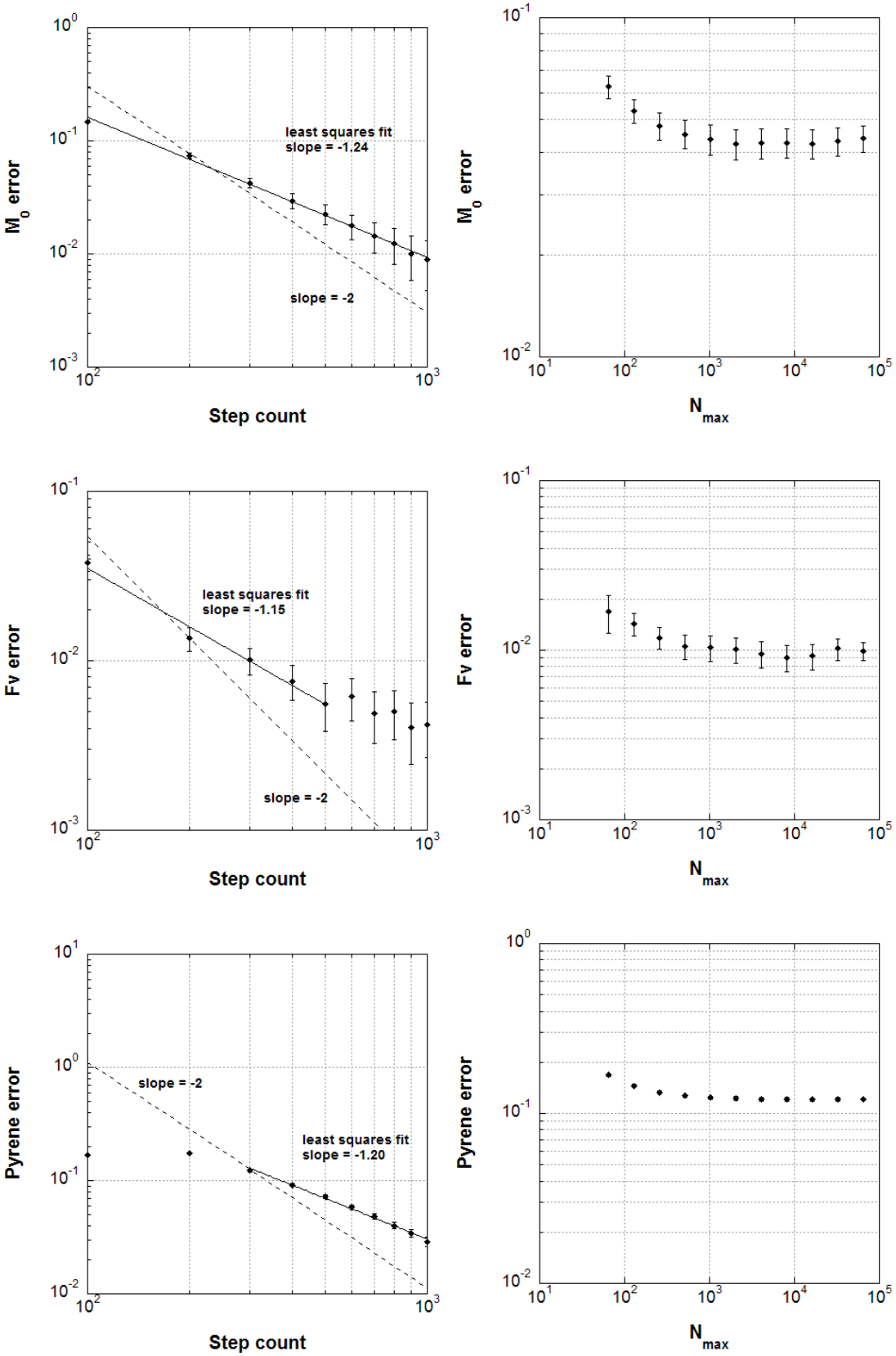

Figure 1: *Order of convergence for a batch reactor.*

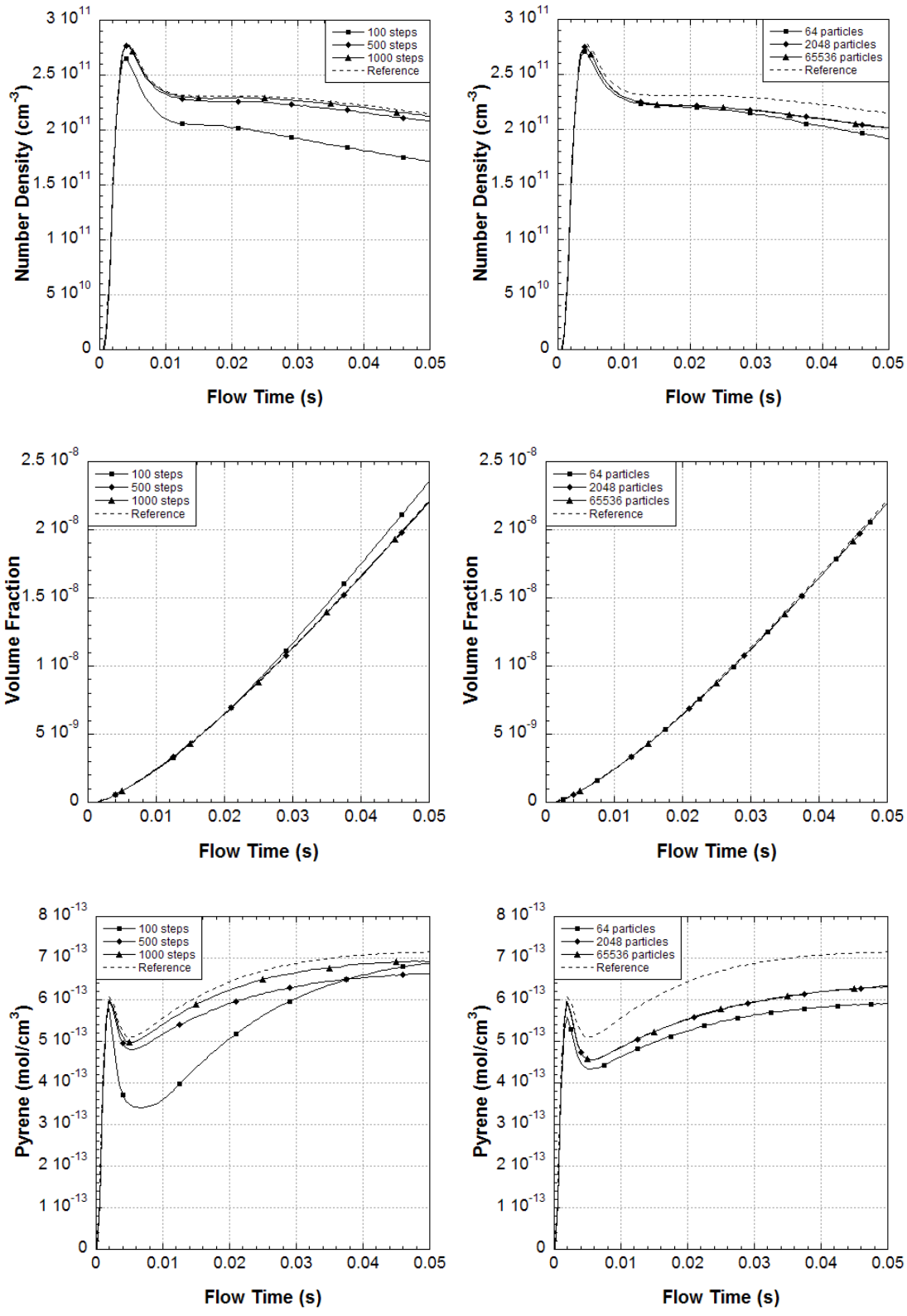

Figure 2: *Transient profiles for a batch reactor. Left column shows behaviour at increasing step count and right column shows behaviour at different stochastic particle counts.*

Figure 2 shows the time evolution of the test variables for the batch reactor. The figure clearly shows the approach towards the reference solution as the step count is increased. F_v converges very quickly and no difference can be seen between the reference case and higher step counts. The figure also shows that, except for the smallest particle count, changing the number of particles does not significantly affect the time profile. This agrees with the only slight change in error seen in figure 1.

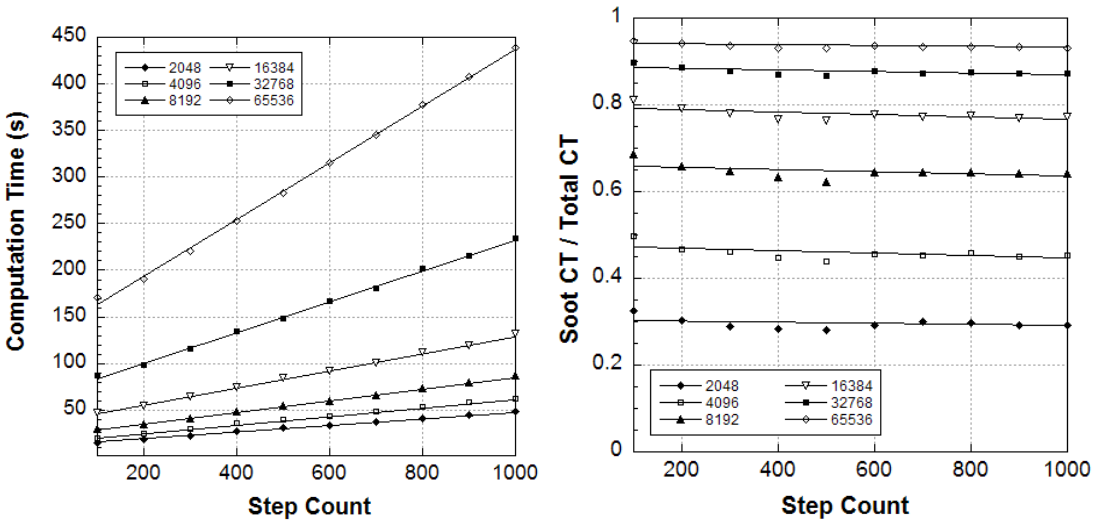

Figure 3: *Single run computation time for a batch reactor.*

The computation time (CT) for a single run is presented in figure 3 for different numerical parameters. The variance in the computation time is very small, and times for different runs do not change by more than about $1 - 2\%$, hence to get the computation time for a simulation merely multiply the number of runs by the times shown in the figure. Computation time is clearly a linear function of step count for the batch reactor. This is intuitive as the more steps that are performed, the more ODE solver initialisations must take place. The computation time also increases with increasing particle count, it would be expected that computation time is proportional to $N \log N$ [25] and this is what is observed here for large N. This behaviour suggests that other factors which affect computation time, such as numerical stiffness of coupling, are not a problem for this test case at all investigated parameters.

4.2 PSR

The PSR test case is an extension of the batch case. The conditions for the PSR test case are the same as the batch case with inflow conditions identical to the initial conditions and a residence time of 5 ms. The simulations are listed in table 2.

The convergence results for the PSR test case are given in figure 4. The figure also shows a least squares power law fit of the data, and unfitted slopes indicating what second order convergence would look like. The PSR exhibits the same behaviour as the batch reactor:

Table 2: *PSR numerical convergence simulations*

Simulation	M	L	N_{max}	Simulation	M	L	N_{max}
1	100	800	2048	11	500	6400	256
2	200	800	2048	12	500	3200	512
3	300	800	2048	13	500	1600	1024
4	400	800	2048	14	500	800	2048
5	500	800	2048	15	500	400	4096
6	600	800	2048	16	500	200	8192
7	700	800	2048	17	500	100	16384
8	800	800	2048	18	500	50	32768
9	900	800	2048	19	500	25	65536
10	1000	800	2048				
Reference Case					2000	50	131072

An continual decrease in error with increasing step count, but no change in error due to increasing particle count. Hence, the PSR has also been shown to converge in this instance. The least squares fits suggest convergence of order 1.6 - 2.2, which is closer to the asymptotic second order convergence found in [23]. The convergence plot for c_{pyr} with step count shows two apparent outlier points as convergence proceeds via a slow, damped oscillation around the reference solution as the step count is increased. This effect can be seen in figure 5.

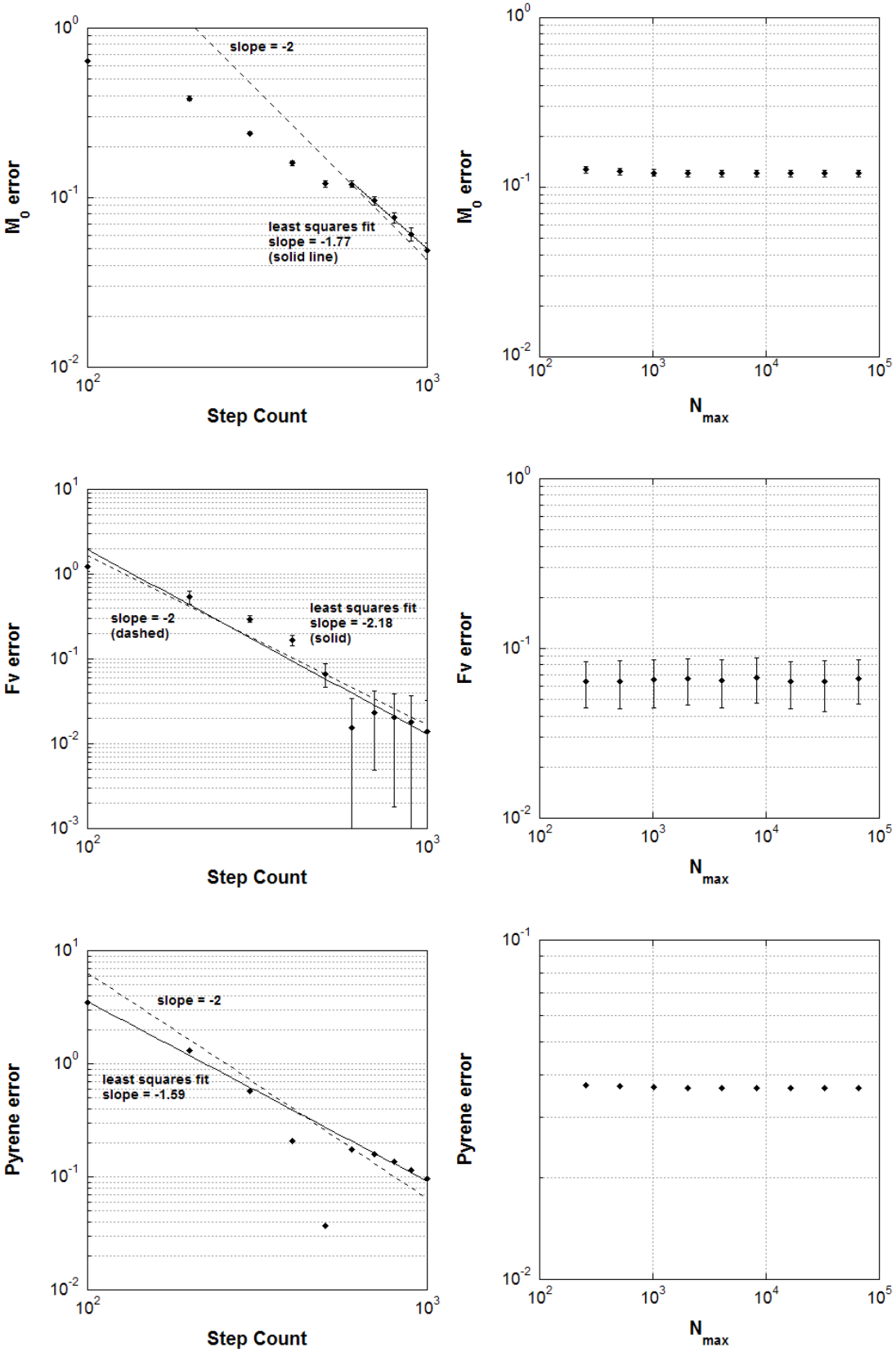

Figure 4: *Order of convergence for the PSR.*

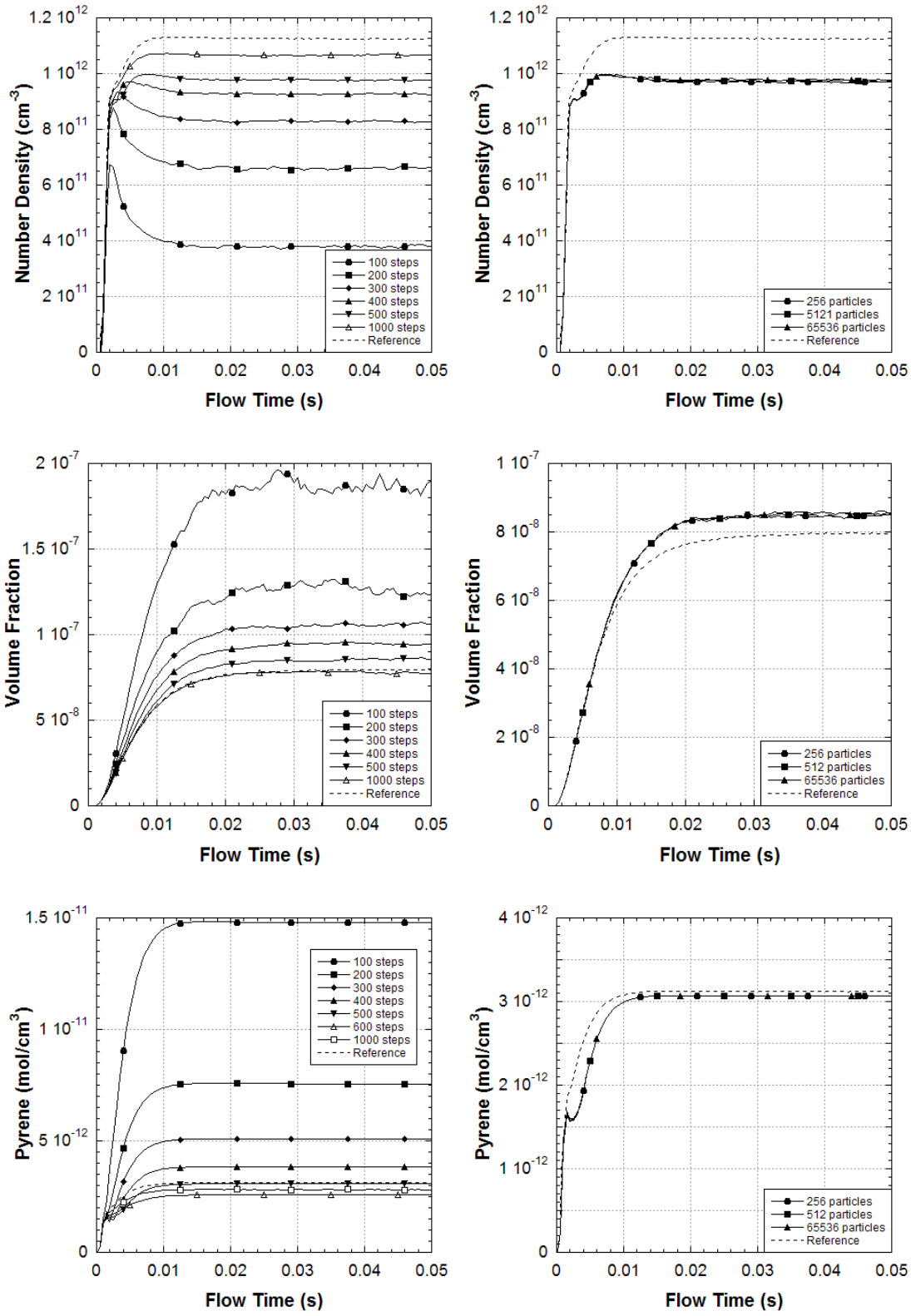

Figure 5: *Transient profiles for the PSR. Left column shows behaviour at increasing step count and right column shows behaviour at different stochastic particle counts.*

Figure 5 shows the time evolution of the test variables for the PSR for different parameters listed in table 2. The left-hand plots clearly show an approach to the reference solution for all variables as the step count is increased. The F_v profile still exhibits statistical fluctuations for low step counts, whereas M_0 and c_{pyr} fluctuate much less at low step counts, even though the absolute value is far from the reference value. A potential explanation for the fluctuation of F_v is the inclusion of a term which removes mass from the soot system (outflow) which is not present in the batch case. Outflow competes with inception and surface growth as the only processes which change mass, however, particles are selected uniformly for removal and a large particle has the same probability of being removed as a small particle. Therefore the PSR simulations are subject to sudden large changes in volume fraction when a particles with masses much larger than the mean are removed. To counter this more simulation runs were performed in order to dampen the fluctuations. The right-hand plots demonstrate that the solution is insensitive to the number of particles, which is in agreement with figure 4.

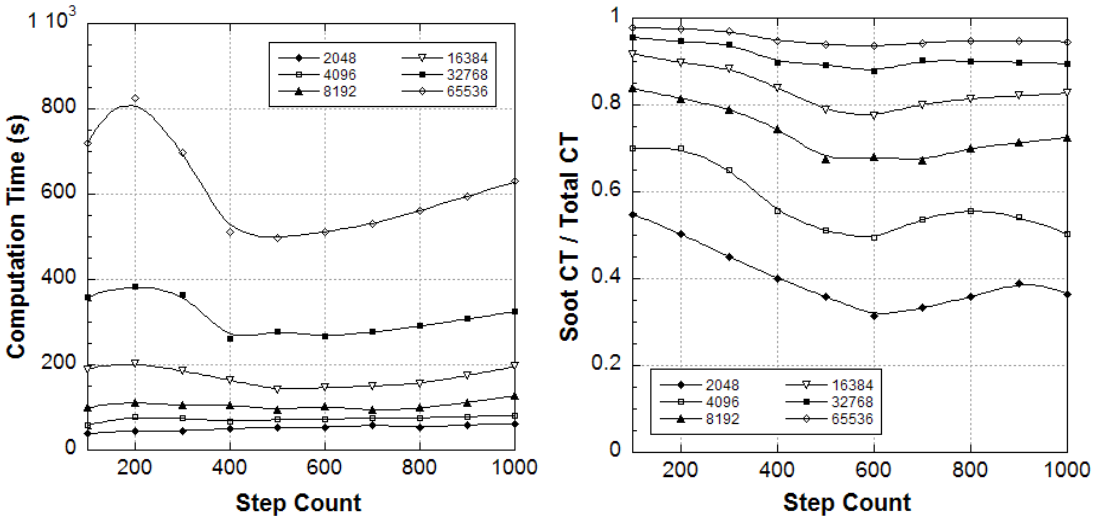

Figure 6: *Single run computation time for a PSR.*

The computation times for the different numerical parameters are shown in figure 6. The left-hand plot suggests there is an increase in computation time low step counts which was not observed for the batch reactor. After the step count has reached about 500 figure 6 shows an approximately linear relationship between step count and computation time, as was observed for the batch reactor. The right-hand graph, showing fraction of computation time spent in the soot solver, shows that the soot solver requires less time overall as the step count approaches 500, after which the fraction of time in the soot solver remains approximately constant.

5 Comparative Cases

5.1 Kronholm Plug-Flow Experiments

Kronholm and Howard [14] used a Jet-Stirred Reactor (JSR) to feed a PFR tube section to give an approximation to plug-flow. This was helped by combusting fuel in the JSR, so that it entered the PFR in equilibrium. [26] demonstrated the application of a moving sectional model to predict Kronholm's experimental results. A stochastic simulation using the method outlined here was performed and compared to the data given by Kronholm and Wen.

The JSR was solved using gas-phase chemistry equations only, as Kronholm does not make mention of soot particles in the JSR. The JSR feed was a C_2H_2/Air mixture with equivalence ratio 2.2. The pressure and temperature were constant at $1\ \mathrm{atm}$ and $1630\ \mathrm{K}$ respectively. The residence time of the JSR was $5.7\ \mathrm{ms}$ [16]. The JSR was solved for a suitably long flow time for the gas to have reached steady-state. The final conditions in the JSR were then used as inputs to the coupled soot algorithm for the PFR. The PFR pressure (constant) and initial temperature were $1\ \mathrm{atm}$ and $1620\ \mathrm{K}$ respectively, and it was solved using the adiabatic energy equation. The PFR was simulated using a maximum of 4096 stochastic particles, 20 runs and 100 steps per millisecond of flow time. Both the spherical particle model and the surface-volume model were used.

Quantities of interest have been plotted along with the experimental results of Kronholm taken from [15, 14] and the sectional method simulation of [26].

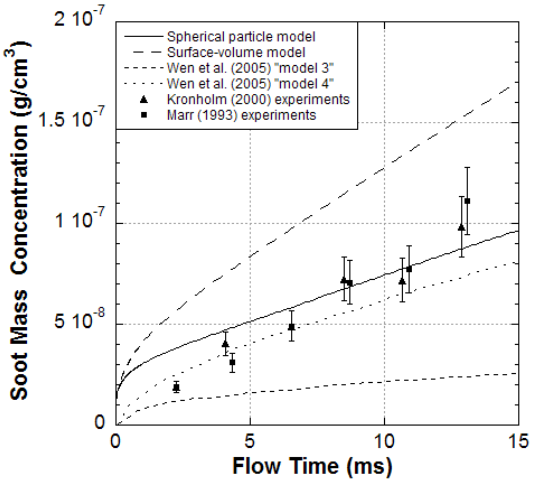

Figure 7: *Soot mass concentration for Kronholm JSR/PFR.*

Figure 7 shows that the stochastic algorithm predicts the soot mass well in both magnitude and transient behaviour. Model "3" by Wen et al. is equivalent to the ABF soot model used for the stochastic study. The difference between Wen et al.'s predictions and ours may be due to them using a constant temperature model and a different soot particle description, whereas we used an adiabatic model. Simulating the PFR as adiabatic was justified be-

cause Kronholm said that the temperature in the PFR changes by about 100 K over the length of the PFR, and this is the change observed in the adiabatic simulations. The prediction is good for the spherical particle model, within experimental error, although the sparsity of experimental data points makes it difficult to draw any firm conclusions.

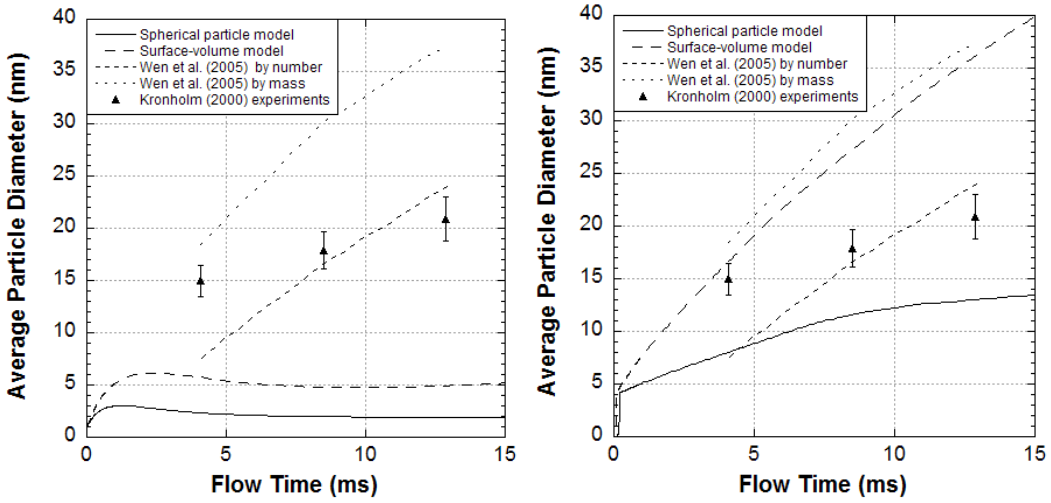

(a) All particles

(b) Particles $> 4\ nm$ diameter

Figure 8: *Average particle diameter for Kronholm JSR/PFR.*

Figure 8 shows the average particle diameter for both particle models along with experimental results and simulations by Wen et al.. There is a poor fit for both particle models with the experimental results when all particles are counted, but the magnitude and slope of the predictions is better if only particles with diameters larger than 4 nm are counted. Figure 8 highlights a caveat in making direct comparisons with the experimental results and stochastic simulations. The stochastic algorithm uses a minimum particle size of 32 carbons atoms (approximately 0.8 nm diameter if the particle is assumed to be spherical). The measuring technique used by Kronholm may not have been able to detect these particles, and hence he measured a much larger average particle size. When the stochastic simulation is plotted without fines (taken as less than 4 nm diameter - empirical estimate) the spherical particle model gives much better agreement with Kronholm's data, and shows a similar trend. The surface-volume model over-predicts the average particle diameter, yet agrees well with the simulations of Wen et al..

Figure 9 shows the time evolution of the PSD for the plug-flow reactor. All particle size distributions were processed using the R statistical software [11]. There is a general good agreement between the spherical particle simulations and the experimental results. However, the simulation seems to continually underpredict the number of particles, and this effect worsens at later times. The simulations also underpredict the peak diameter slightly, though this effect diminishes at later times. The surface-volume model does not exhibit the same particle distribution as the experiments, grossly underpredicts particle number density and shows far more larger particles. Interestingly, Kronholm's data shows no particles at under about 6 nm, which lends justification to the decision to discount particles

smaller than $4\ \mathrm{nm}$ from the calculation of the mean. Figure 9(b) shows more clearly the bimodal nature of the predicted distributions, in particular the very large number of small particles.

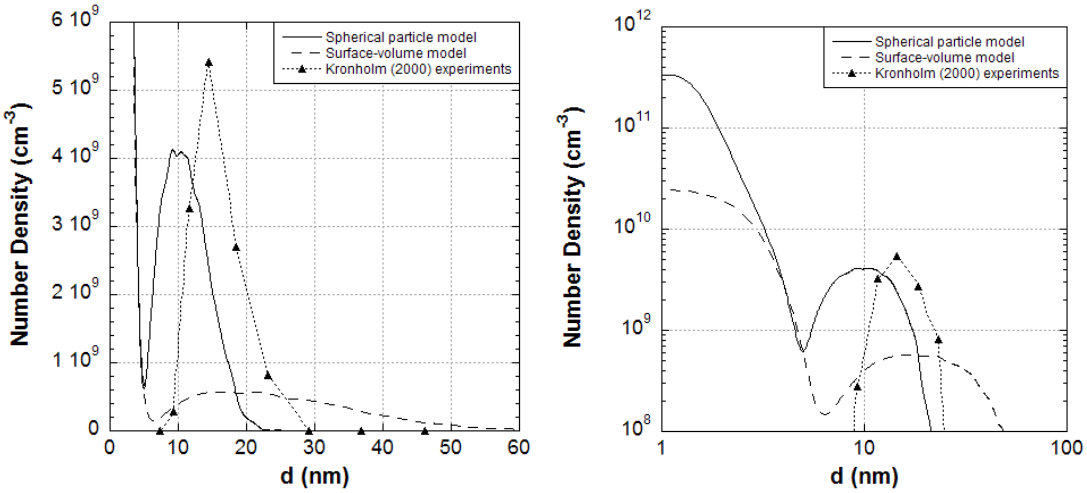

(a) 7.6 ms

(b) 7.6 ms (log scale)

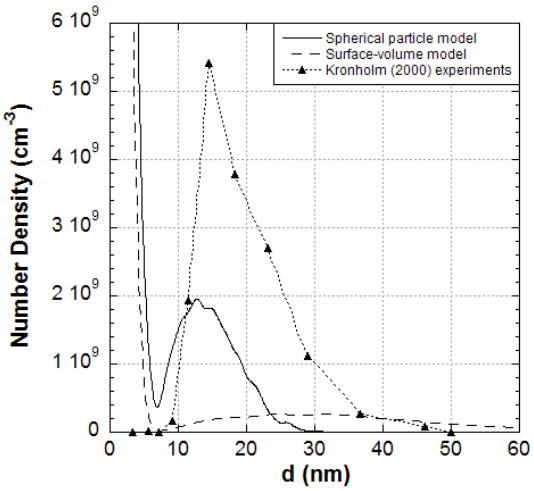

(c) 12.0 ms

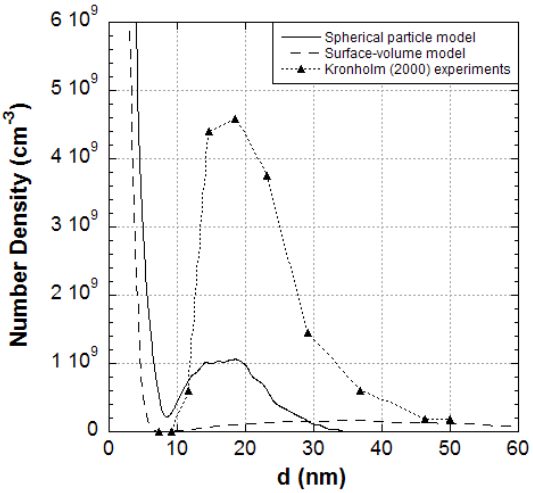

(d) 16.4 ms

Figure 9: *Particle size distributions for Kronholm JSR/PFR.*

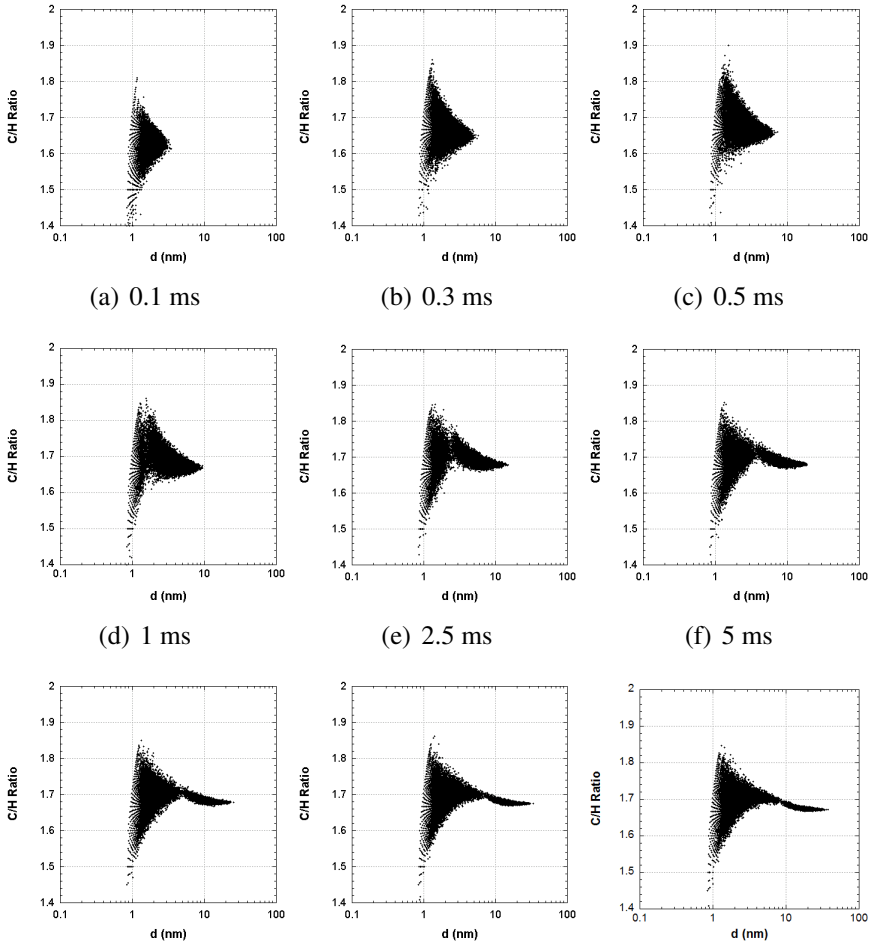

(a) 0.1 ms (b) 0.3 ms (c) 0.5 ms

(d) 1 ms (e) 2.5 ms (f) 5 ms

(g) 7.6 ms (h) 12 ms (i) 16.4 ms

Figure 10: *C/H ratio scatter plots for spherical particle model.*

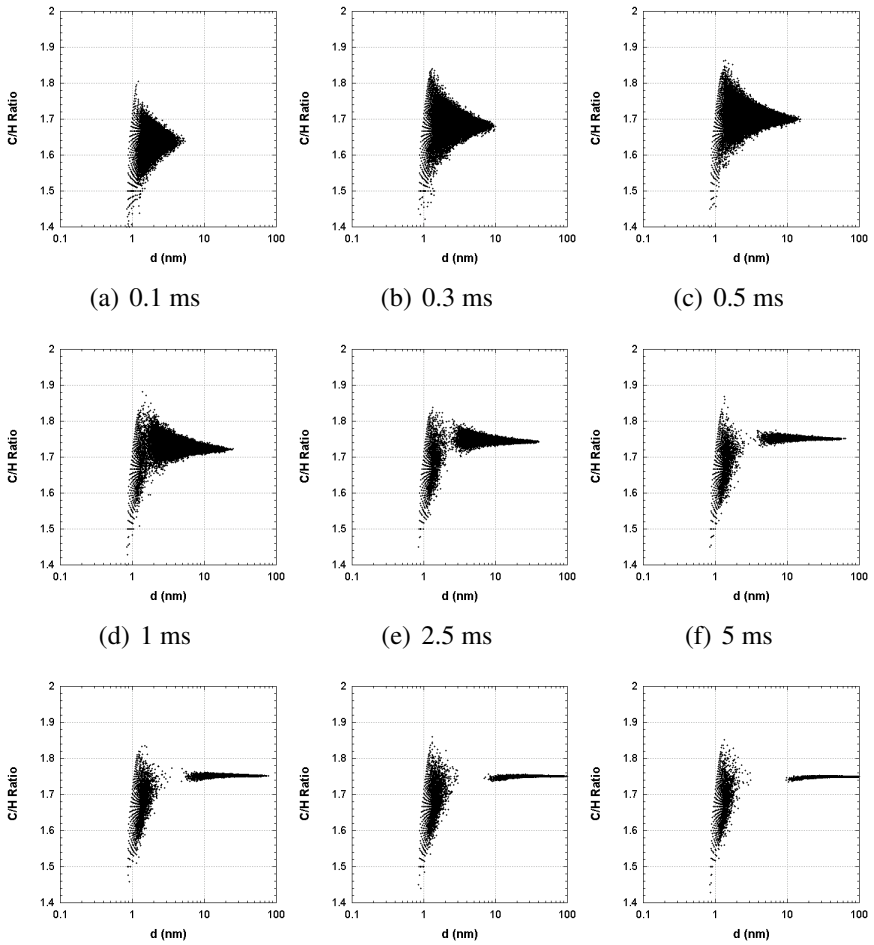

(a) 0.1 ms (b) 0.3 ms (c) 0.5 ms

(d) 1 ms (e) 2.5 ms (f) 5 ms

(g) 7.6 ms (h) 12 ms (i) 16.4 ms

Figure 11: *C/H ratio scatter plots for surface-volume model.*

Unlike the other techniques, the stochastic technique allows the composition of the particulate matter to be tracked explicitly. Figures 10 and 11 show the carbon to hydrogen (C/H) ratio of each particle plotted against particle diameter. It shows that small particles exhibit a wider range of compositions than larger particles. For the ABF model the two main growth processes are C_2H_2 addition and pyrene condensation. C_2H_2 adds carbon and hydrogen in the ratio $2 : 1$ whereas pyrene adds in the ratio $1.6 : 1$, therefore it would be expected to observe particle compositions between these values. This is exactly what we see from these figures. Initially the C/H ratio increases slowly suggesting that the HACA mechanism becomes dominant over condensation and inception. Larger particles show a narrower range of compositions, in particular for the surface-volume model. This is because surface processes do not alter the number of carbon and hydrogen atoms greatly relative to the total number in larger particles, for example a spherical particle of diameter 60 nm will contain over ten million carbon atoms.

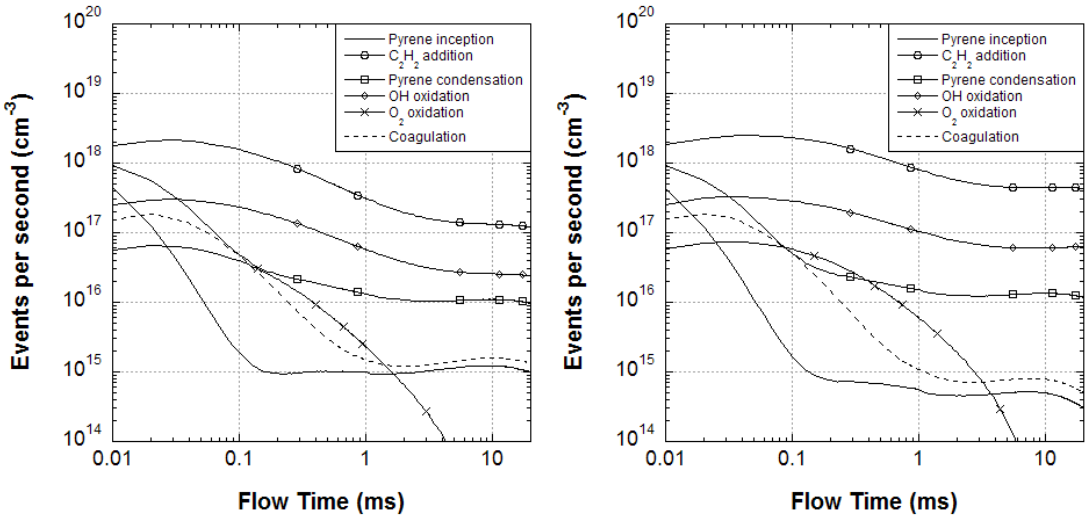

(a) Spherical particle model (b) Surface-volume model

Figure 12: *Soot process rates.*

The rates of all soot processes are given in figure 12. At early times there is little difference between the two models. However, the surface-volume model clearly shows a higher C_2H_2 addition rate at later times. The pyrene condensation rate remains similar throughout for both models. This accounts for the higher overall C/H ratios observed for the surface-volume model in figure 11. The surface-volume model predicts a much higher surface area than the spherical particle model, which accounts for the higher acetylene rate.

Figure 13 shows the difference in soot surface area over time for both particle models. The surface-volume model clearly predicts a larger surface area than the spherical particle model; after 20 ms flow time the difference is almost five times. This accounts for the increased surface rates in figure 12 and hence the larger particles predicted by the surface-volume model.

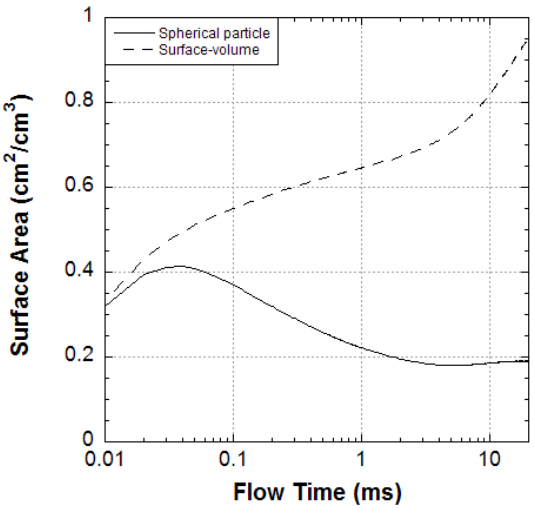

Figure 13: *Soot surface area.*

5.2 Perfect Stirred Reactor Model

Despite potential instabilities in the algorithm for a PSR it was decided to simulate a PSR to see if physically meaningful predictions could be achieved. No experimental studies of soot formation in a PSR could be found for comparison, but an earlier method of moments study [5] has been done. This study was repeated using the currently available chemistry mechanisms and the predictions were compared to the new predictions using the coupled stochastic solver. The solution parameters were 1000 splitting steps, 4096 stochastic particles and 20 runs for $0.12\,\mathrm{atm}$ and $1\,\mathrm{atm}$, and 100 runs for $10\,\mathrm{atm}$. 10 steps were used per millisecond of flow time. Plots of volume fraction (figure 14), aromatics concentrations (figure 15) and surface process rates (figure 16) are given here.

Figure 14 shows that the stochastic technique and the method of moments agree well for $0.12\ \mathrm{atm}$ and $1\ \mathrm{atm}$, but at $10\ \mathrm{atm}$ there is less agreement. In the method of moments additional approximations have to be made in order to solve in the transition regime [13]. These approximations are not required for the stochastic simulations, which might explain the discrepancy. The transient plot (right-hand) appears to back up this conclusion, showing a fluctuating solution.

Figures 15 and 16 show results at $1\ \mathrm{atm}$ only. Figure 15 demonstrates excellent agreement between the two solution methods for the prediction of smaller aromatic species. Figure 16 shows the surface process rates for both solution methods. Due to the nature of the stochastic algorithm and the linear process deferment [18], the surface rates predicted by the stochastic solver are estimates, though they still show good agreement with the method of moments.

The comparison between the method of moments and the coupled stochastic algorithm demonstrates that despite the numerical instabilities in the explicit stochastic solver, it is still capable of predicting as well as the implicit method of moments solver.

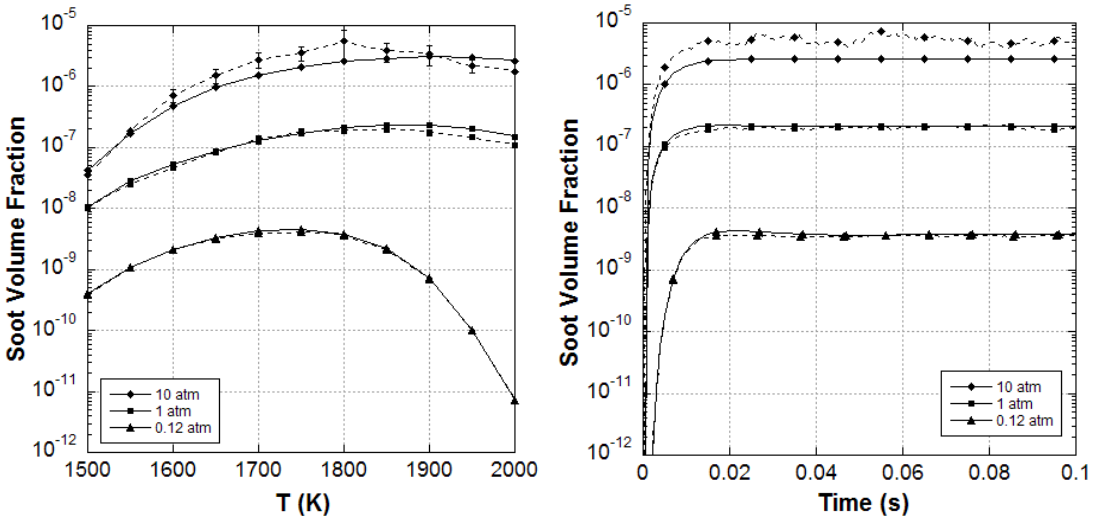

Figure 14: *Volume fractions from Brown et al. for method of moments (solid) and stochastic (dotted) PSR simulations. Right-hand graph shows the transient behaviour at* 1800 K.

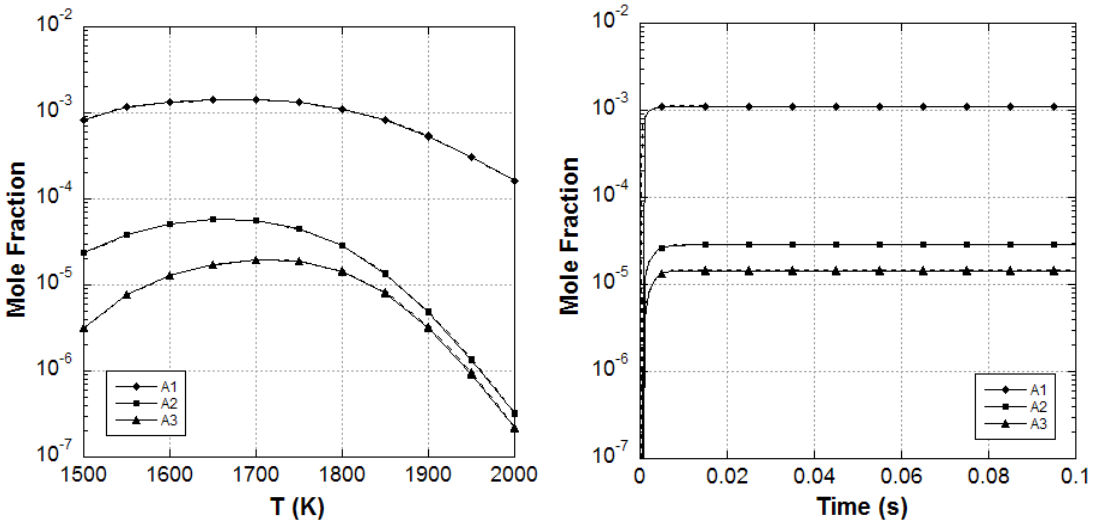

Figure 15: *PAH concentrations from Brown et al. for method of moments (solid) and stochastic (dotted) simulations. Right-hand graph shows the transient behaviour at* 1800 K.

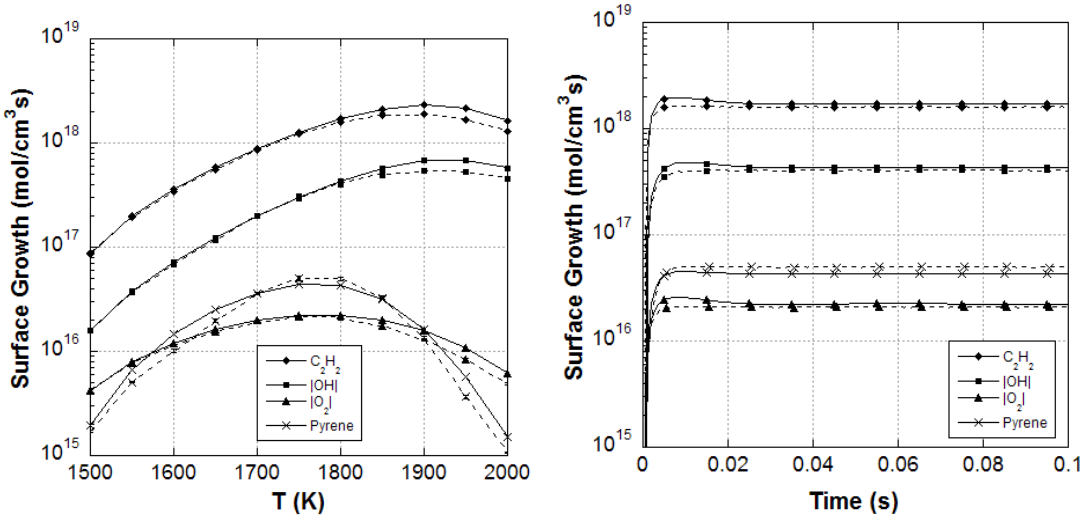

Figure 16: *Surface rates from Brown et al. for method of moments (solid) and stochastic (dotted) simulations. Right-hand graph shows the transient behaviour at* 1800 K.

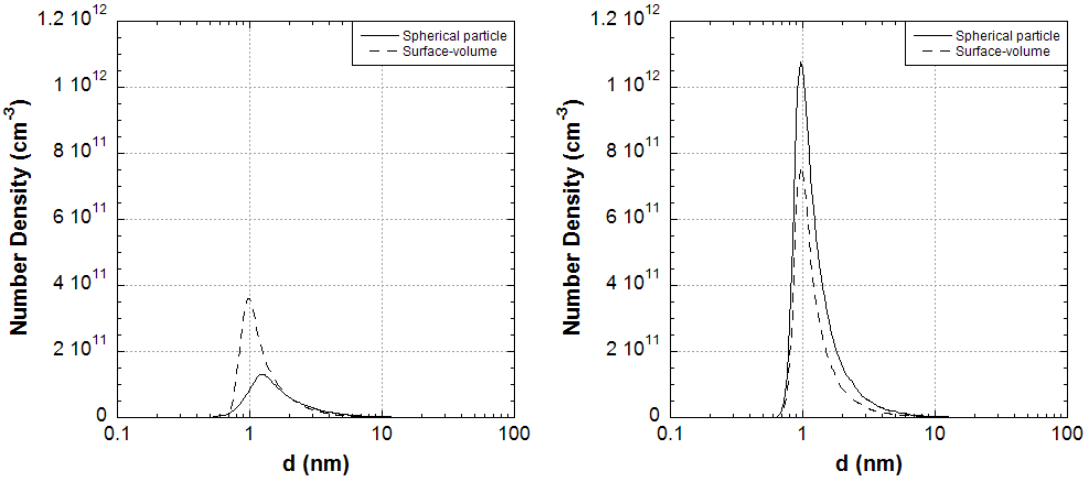

(a) 1500 K (b) 1600 K

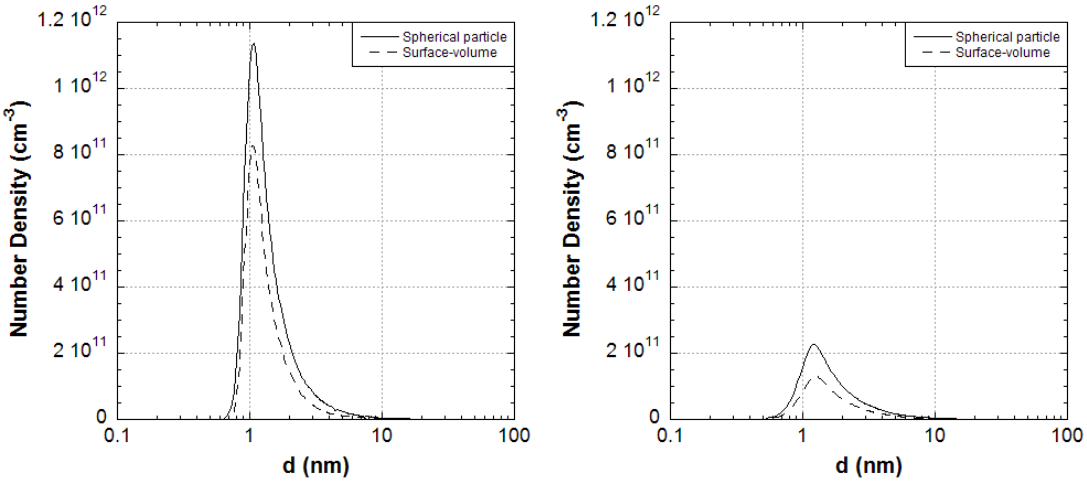

(c) 1700 K (d) 1900 K

Figure 17: *Particle size distributions predicted in PSR.*

Figure 17 shows the particle size distribution in the PSR for both the spherical particle and the surface-volume model at $100\ \mathrm{ms}$ flow time for the $1\ \mathrm{atm}$ case. Unlike the PFR, there is a good agreement between the two models for particle shape, with the mean size appearing around $1\ \mathrm{nm}$ diameter. This is expected because with such small particles aggregates cannot have formed, and hence there should be little difference between the two models. The distributions are unimodal, where the PFR distributions were bimodal. The unimodality helps explain the close agreement between the stochastic simulation and the method of moments at low pressure, as the method of moments is better suited to such systems. There is also good agreement in number density between the models, with the spherical particle model predicting more particles except at lower temperatures.

6 Conclusions

A numerical convergence study has been perform for a stochastic soot balance coupled to gas-phase chemistry. Two systems were investigated; a batch reactor and a PSR. Both were found to converge numerically with splitting step size. However, the PSR was found to exhibit numerical instabilities for certain numerical parameters, which might be due to stiffness of the coupling. This warrants further investigation.

Comparison to the plug flow reactor experiments of [15] and [17] demonstrated good agreement. There were some deviations of the simulation predictions from the experimental results for mean particle diameter, which could be the result of limited particle detection of the experiments, limitations of the ABF soot mechanism, or a problem of the algorithm. A study of carbon to hydrogen ratio in soot particles in the PFR was presented for the first time which demonstrated that the model predicts C/H ratio to increase over time and that larger particles occupy a narrower range of compositions.

A PSR simulation was performed and compared to a similar method of moments simulation reported in [5]. Again good agreement between the two simulation methods adds weight to the validity of this solution approach. However, lack of experimental evidence for soot formation in a PSR precludes further conclusions to be drawn as to the suitability of the algorithm in such systems, especially with the observed instabilities of solution. The PSD for soot in a PSR have been shown for the first time.

7 Acknowledgments

This work was funded by an EPSRC DTA and was completed at the department of chemical engineering at the University of Cambridge, UK.

References

[1] J Appel, H Bockhorn, and M Frenklach. Kinetic modeling of soot formation with detailed chemistry and physics: Laminar premixed flames of C_2 hydrocarbons. Combust. Flame, 121:122–136, 2000.

[2] Jrg Appel, Henning Bockhorn, and Michael Wulkow. A detailed numerical study of the evolution of soot particle size distributions in laminar premixed flames. Chemosphere, 42:635–645, 2001.

[3] M Balthasar and M Kraft. A stochastic approach to solve the particle size distribution function of soot particles in laminar premixed flames. Combust. Flame, 133:289–298, 2003.

[4] K E Brenan, S L Campbell, and L R Petzold. Numerical solution of initial-value problems in differential-algebraic equations. SIAM Classics in Applied Mathematics, 14, 1996.

[5] Nancy J Brown, Kennath L Revzan, and Michael Frenklach. Detailed kinetic modelling of soot formation in ethylene/air mixtures reacting in a perfectly stirred reactor. Proc. Comb. Inst., 27:1573–1580, 1998.

[6] J R Cash. Efficient numerical methods for the solution of stiff initial-value problems and differential algebraic equations. Proc. Royal Soc. London, 459:797–815, 2003.

[7] A Eibeck and W Wagner. Stochastic interacting particle systems and nonlinear kinetic equations. Ann. Appl. Probab., 13(3):845–889, 2003.

[8] Michael Frenklach. Method of moments with interpolative closure. Chem. Eng. Sci, 57:2229–2239, 2002.

[9] Michael Frenklach and Hai Wang. Detailed modelling of soot particle nucleation and growth. Proc. Comb. Inst., 23:1559–1566, 1990.

[10] Michael Frenklach and Hai Wang. Detailed Mechanism and Modelling of Soot Particle Formation, volume 59 of Series in Chemical Physics, pages 162–190. Springer Verlag, Berlin, 1994.

[11] Robert Gentleman and Ross Ihaka. R statistical software, 2005. www.r-project.org.

[12] E Hairer and G Wanner. Solving Ordinary Differential Equations II. Stiff and Differential-Algebraic Problems. Springer Verlag, 1996.

[13] A Kazakov and M Frenklach. Dynamic modeling of soot particle coagulation and aggregation: Implementation with the method of moments and application to high-pressure laminar premixed flames. Combust. Flame, 114:484–501, 1998.

[14] David F Kronholm and Jack B Howard. Analysis of soot surface growth pathways using published pfr data with new psd measurements and published premixed flame data. Proc. Comb. Inst., 28:2555–2561, 2000.

[15] David Franklin Kronholm. Molecular Growth Pathways in Fuel-Rich Combustion. PhD thesis, Massachusetts Institute of Technology, 2000.

[16] Frederick W Lam, Jack B Howard, and John P Longwell. The behaviour of polycyclic aromatic hydrocarbons during the early stages of soot formation. Proc. Comb. Inst., 22:323–332, 1989.

[17] J A Marr. PhD thesis, Massachusetts Institute of Technology, 1993.

[18] Robert Patterson, Jasdeep Singh, Michael Balthasar, Markus Kraft, and James Norris. The Linear Process Deferment Algorithm: A new technique for solving population balance equations. SIAM Journal on Scientific Computing, (28):303–320, 2006.

[19] Robert Patterson, Jasdeep Singh, Neal Morgan, and Markus Kraft. A simple model for the aggregate structure of soot particles. Technical Report 38, c4e Preprint-Series, Cambridge, 2006.

[20] Henning Richter, Silvia Granata, William Green, and Jack Howard. Detailed modelling of pah and soot formation in a laminar premixed benzene/oxygen/argon low-pressure flame. Proc. Comb. Inst., 30:1397–1405, 2005.

[21] K K Sabelfeld, S V Rogasinsky, A A Kolodko, and A I Levykin. Stochastic algorithms for solving Smoluchovsky coagulation equation and applications to aerosol growth simulation. Monte Carlo Methods and Appl., 2(1):41–87, 1996.

[22] J Singh, R Patterson, M Balthasar, M Kraft, and W Wagner. Modelling soot particle size distribution: Dynamics of pressure regimes. Technical Report 25, c4e Preprint-Series, Cambridge, 2004.

[23] Gilbert Strang. On the construction and comparison of difference schemes. SIAM Journal of Numerical Analysis, 5(3):506–517, 1968.

[24] Hai Wang and Michael Frenklach. A detailed kinetic modelling study of aromatic formation in laminar premixed acetylene and ethylene flames. Combust. Flame, 110:173–221, 1997.

[25] Clive Wells and Markus Kraft. Direct simulation and mass flow stochastic algorithms to solve a sintering-coagulation equation. Monte Carlo Methods and Appl., 11(2):175–199, 2005.

[26] John Z. Wen, M.J. Thomson, S.H. Park, S.N. Rogak, and M.F. Lightstone. Study of soot growth in a plug flow reactor using a moving sectional model. Proc. Comb. Inst., 30:1477–1484, 2005.

[27] B Yang and S B Pope. An investigation of the accuracy of manifold methods and splitting schemes in the computational implementation of combustion chemistry. Combust. Flame, 112:16–32, 1998.